



Article

Synergistic Antitumor Effects of ^{177}Lu -Octreotide Combined with an ALK Inhibitor in a High-Risk Neuroblastoma Xenograft Model

Arman Romiani ^{1,2} , Daniella Pettersson ^{1,2}, Nishte Rassol ^{1,2}, Klara Simonsson ^{1,2}, Hana Bakr ^{1,2,3}, Dan E. Lind ^{2,4} , Anikó Kovács ^{2,5} , Johan Spetz ^{1,2} , Ruth H. Palmer ^{2,4} , Bengt Hallberg ^{2,4} , Khalil Helou ^{2,6} and Eva Forssell-Aronsson ^{1,2,3,*}

- ¹ Department of Medical Radiation Sciences, Institute of Clinical Sciences, Sahlgrenska Academy, University of Gothenburg, Sahlgrenska University Hospital, SE-41345 Gothenburg, Sweden; arman_romiani@hotmail.com (A.R.); daniella.pettersson@vgregion.se (D.P.); nishte.rassol@gu.se (N.R.); klara.simonsson@regionstockholm.se (K.S.); hana.bakr@gu.se (H.B.); johan.spetz@gu.se (J.S.)
 - ² Sahlgrenska Center for Cancer Research, Sahlgrenska Academy, University of Gothenburg, Box 425, SE-40530 Gothenburg, Sweden; aniko.kovacs@vgregion.se (A.K.); khalil.helou@oncology.gu.se (K.H.)
 - ³ Medical Physics and Biomedical Engineering, Sahlgrenska University Hospital, SE-41345 Gothenburg, Sweden
 - ⁴ Department of Medical Biochemistry and Cell Biology, Institute of Biomedicine, Sahlgrenska Academy, University of Gothenburg, SE-41390 Gothenburg, Sweden; dan.emil.lind@gu.se (D.E.L.); ruth.palmer@gu.se (R.H.P.); bengt.hallberg@gu.se (B.H.)
 - ⁵ Department of Clinical Pathology, Institute of Clinical Sciences, Sahlgrenska Academy, University of Gothenburg, Sahlgrenska University Hospital, SE-41345 Gothenburg, Sweden
 - ⁶ Department of Oncology, Institute of Clinical Sciences, Sahlgrenska Academy, University of Gothenburg, Sahlgrenska University Hospital, SE-41345 Gothenburg, Sweden
- * Correspondence: eva.forssell_aronsson@radfys.gu.se



Citation: Romiani, A.; Pettersson, D.; Rassol, N.; Simonsson, K.; Bakr, H.; Lind, D.E.; Kovács, A.; Spetz, J.; Palmer, R.H.; Hallberg, B.; et al. Synergistic Antitumor Effects of ^{177}Lu -Octreotide Combined with an ALK Inhibitor in a High-Risk Neuroblastoma Xenograft Model. *Therapeutics* **2024**, *1*, 4–21. <https://doi.org/10.3390/therapeutics1010003>

Academic Editor: Aurel Popa-Wagner

Received: 24 May 2024

Revised: 13 July 2024

Accepted: 29 July 2024

Published: 7 August 2024



Copyright: © 2024 by the authors. Licensee MDPI, Basel, Switzerland. This article is an open access article distributed under the terms and conditions of the Creative Commons Attribution (CC BY) license (<https://creativecommons.org/licenses/by/4.0/>).

Abstract: Background/Objectives: Neuroblastoma (NB) is a childhood cancer with heterogeneous characteristics, posing challenges to effective treatment. NBs express somatostatin receptors that facilitate the use of somatostatin analogs (SSTAs) as tumor-seeking agents for diagnosis and therapy. High-risk (HR) NBs often have gain-of-function mutations in the receptor tyrosine kinase anaplastic lymphoma kinase (ALK). Despite intensive multimodal treatment, survival rates remain below 40% for children with HR-NB. The aim of this work was to investigate the combined effect of the SSTA ^{177}Lu -octreotide with the ALK inhibitor lorlatinib. **Methods:** Mice bearing human HR-NB CLB-BAR tumors were treated with lorlatinib, ^{177}Lu -octreotide, and a combination of these pharmaceuticals or saline (control). Tumor volume was monitored and tumor samples were evaluated for cleaved caspase-3 and expression of 84 human genes involved in apoptosis. **Results:** Combination treatment with ^{177}Lu -octreotide and lorlatinib demonstrated synergistic antitumor effects. An increased number of cleaved caspase 3-positive cells was observed in tumors from mice treated with ^{177}Lu -octreotide alone and in combination with lorlatinib. Modulation of Bcl-2 family gene expression was observed only in the presence of both ^{177}Lu -octreotide and lorlatinib, with BID down-regulated and HRK up-regulated on days 2 and 7, respectively. **Conclusions:** The data suggest that ALK signaling pathway inhibition may contribute to radiosensitization in radionuclide therapy with ^{177}Lu -octreotide and could improve treatment outcomes in patients with HR-NB.

Keywords: neuroblastoma; radionuclide therapy; apoptosis; somatostatin analog; ALK-inhibitor; radiosensitization

1. Introduction

Anaplastic lymphoma kinase (ALK) is a receptor tyrosine kinase (RTK), a member of the insulin RTK family, which is expressed in the developing central and peripheral nervous system [1]. ALK dimerization, in response to ALK in vivo ligand (ALKAL) binding,

activates signaling pathways involved in various cellular processes, such as proliferation, transcription, growth, and survival [1]. Mutated, rearranged, or amplified *ALK* in a wide range of tumors acts as an oncogene. *ALK* overexpression has been identified in several tumor types, including ovarian cancer, breast cancer, and neuroblastoma (NB). Among newly diagnosed high-risk (HR) NB patients, *ALK* mutations or gene amplification occur in approximately 14% [2–4]. Excess of the transcription factor MYCN is associated with several tumor types, but especially NBs, and previous studies have illustrated the cooperativity of *ALK* and MYCN, the major oncoprotein of HR-NB [5–7]. Despite intensive multimodal treatment, and significant improvements, survival rates remain less than 40% for children with HR-NB [8].

Lorlatinib is a potent *ALK* inhibitor (*ALKi*) that binds to the ATP binding site of the *ALK* kinase domain, preventing *ALK* downstream signaling [9]. Lorlatinib was FDA approved in 2018 for treatment of *ALK*-positive metastatic non-small-cell lung cancer and has demonstrated robust antitumor effects in comparison with other *ALKis* [10–12]. Classified as a third-generation *ALKi*, lorlatinib demonstrates activity against several drug-resistant *ALK* mutations [11]. Phase I trials have been reported in patients with *ALK*-positive NB, both as monotherapy and in combination, with manageable toxicity profiles and antitumor effects [13,14]. Despite this, studies suggest that treatment with lorlatinib can still lead to drug resistance [15–18], strengthening the need to understand the underlying mechanisms of drug resistance and highlighting the need to identify combination therapy options.

^{177}Lu -[DOTA^o, Tyr³]octreotide (^{177}Lu -octreotide) is a radiopharmaceutical that binds to somatostatin receptors (SSTRs) [19–21]. Octreotide is a synthetic somatostatin analog (SSTA) with high affinity for SSTR2 [22]. ^{177}Lu is a beta-emitting radionuclide with a half-life of 6.7 days. The range of the emitted electrons ($E_{\beta\text{max}} = 497 \text{ keV}$) is <2 mm in tissue, which is well suited for disseminated tumors [23–25]. The closely related radiopharmaceutical, ^{177}Lu -octreotate, is FDA and EMA approved for treatment of gastroenteropancreatic neuroendocrine tumors. Previous preclinical and clinical studies have demonstrated selective uptake and therapeutic potential from the use of radiolabeled SSTAs for SSTR-positive HR-NB; however, the modest therapy effect in some of the studies highlights the need for optimization of these treatments [26–29]. An ongoing phase II study with ^{177}Lu -octreotate is now being conducted where an individualized treatment regimen is reviewed for children with relapsed HR-NB (neuroblastoma-LuDO-N) [30].

New treatment strategies are required to increase the cure rate in HR-NB. One proposed option for optimization of radiolabeled SSTA therapy could be to administer it in combination with another drug, in order to increase the effect on tumor tissue [31]. This increased effect could be mediated through specific drug–drug interactions or by independent, additive effects. With the treatment-resistance properties of HR-NB, combination treatments with radionuclide therapy and *ALKi* could be beneficial. The aim of this work was to examine the effects of combination treatment with lorlatinib and ^{177}Lu -octreotide on growth and expression of apoptosis-related genes in the tumors of NB-bearing mice.

2. Materials and Methods

2.1. Tumor Cell Line and Animal Model

The study was performed with CLB-BAR (*ALK* gain of function, *exon4–11* truncated *ALK*; MYCN amplification) NB cells obtained from The Center Leon Berard, France under MTA [32]. The CLB-BAR cell line was established from a stage 4 NB tumor at relapse for a female child, after the consent of her parents. Approval of care and use of these samples was given by the Biological Resources Center Ethical and Steering committees of Centre Léon Bérard and Institut Gustave Roussy.

CLB-BAR cells were cultured as previously described [26]. A mixture of Matrigel (354248, Corning, New York, NY, USA) and 1.5×10^6 CLB-BAR cells were injected s.c. into the flank of 5–6-week-old female BALB/c nude mice (Janvier Labs, Saint-Berthevin, France), after acclimatization for 1 week after delivery to the Experimental Biomedicine Lab at University of Gothenburg. All animal experiments were approved by the Swedish Ethical

Committee on Animal Experiments in Gothenburg (ethical reference number 2779-20) and carried out following guidelines from Animal Research: Reporting of In Vivo Experiments (ARRIVE).

2.2. Pharmaceuticals

Lorlatinib (S7536, Selleckchem, Houston, TX, USA) was formulated in 2% DMSO, 30% PEG300, and double-distilled water. The solution was prepared for oral gavage with 10 mg/kg for each mouse.

^{177}Lu -octreotide was prepared according to the manufacturer's requirements (ITG Isotope Technologies Garching GmbH, Munich, Germany). Instant thin layer chromatography (ITLC-SG, chromatography paper 50/PK, Varian Medical Systems, Palo Alto, CA, USA), with 0.1 M of sodium citrate as the mobile phase, was implemented to determine the radiochemical purity, which was above 97%. The specific activity of ^{177}Lu -octreotide was 66 MBq/ μg , yielding approximately 0.47 μg peptide for 30 MBq ^{177}Lu -octreotide. ^{177}Lu activity in each syringe was measured with an ionization chamber with a ^{177}Lu energy window setting (CRC-15R, Capintec, Inc., Florham Park, NJ, USA) before and after injection, and by subtracting the remaining activity after injection from the activity before injection, the actual administered activity to each mouse was determined.

2.3. Treatment Regimens

Tumor-bearing mice were divided into four groups ($n = 10$ mice/group) aiming for as similar a tumor volume distribution as possible between groups. Mean tumor volume was 480 mm³ (SEM = 30 mm³) at treatment start. Mice in the groups were treated with either (1) lorlatinib via daily oral gavage (10 mg/kg body weight) (from day 0 to day 14), (2) with a single i.v. injection with 30 MBq ^{177}Lu -octreotide on day 1, or (3) a combination of both treatments. The fourth group acted as a control and received an i.v. injection with saline on day 1.

Mouse weight and tumor volume was measured four times per week. Tumor volume, V , was calculated based on measurements using digital calipers of the three perpendicular axes (a , b , and c) of the tumor: $V = \frac{4\pi abc}{3}$.

Three mice from each group were sacrificed on day 2 and three on day 7, and the remaining four mice in each group on day 14. At sacrifice, the animals were under anesthesia with pentobarbitalnatrium (vet. 60 mg/mL, Apotek Produktion & Laboratorier AB, Kungens kurva, Sweden) injected i.p. before cardiac puncture. Tumor samples from each time point (days 2, 7, and 14) were collected and divided into two parts, one placed in vials with formalin for immunohistochemical (IHC) analysis and the other freshly frozen in liquid nitrogen and stored at -80°C for real-time reverse transcription polymerase chain reaction (qPCR) analysis.

2.4. Immunohistochemical Analysis

After fixation in formalin, tumor samples were embedded in paraffin, sectioned (thickness 4 μm), deparaffinized, rehydrated, and pretreated using the Dako PTLINK system (Dako, Carpinteria, CA, USA) and processed on an automated DAKO Autostainer platform using the DAKO EnVision[®] FLEX High pH Link kit (pH 9) [26]. IHC staining was performed with anti-cleaved caspase-3 (CC3) (1:100, #9661, Cell Signaling Technology, Beverly, MA, USA) according to the procedure proposed by the manufacturer. Counterstaining was made with hematoxylin. Slowly growing NB tissue was used as the negative control, and irradiated NB tissue was used as the positive control. Digital images were captured with a 40 \times magnification using a Panoramic Scanner P250 (3DHISTECH, Budapest, Hungary) at Histocenter AB (Möln dal, Sweden), with the software CaseViewer 2.4, Slide Converter.

For a quantitative representation of the IHC data, IHC scoring was performed by a certified and experienced pathologist using the semi-quantitative HistoScore method, where

$$\text{HistoScore} = ((1 \times \% \text{ weak}) + (2 \times \% \text{ moderate}) + (3 \times \% \text{ strong})) \quad (1)$$

was calculated based on visual (eyeballing) assessment of the intensity of the staining (graded: 0, negative; 1, weak; 2, moderate; or 3, strong) and the percentage of positive cells within each entire section.

2.5. Gene Expression Analyses

RNA was extracted from tumor samples using a phenol-chloroform method (RNeasy Lipid Tissue Mini Kit, QIAGEN, Valencia, CA, USA). RNA purity, integrity, and concentration were assessed with a Nanodrop 1000 Spectrometer (Thermo Fisher Scientific, Waltham, MA, USA) ($260/280 > 1.8$), Agilent 2100 Bioanalyzer (Agilent Technologies, Santa Clara, CA, USA) ($RIN > 8$), and a Qubit 3.0 Fluorometer (Thermo Fisher Scientific, Waltham, MA, USA), respectively. cDNA was subsequently generated via reverse transcription (RT² First Strand Kit, QIAGEN, Valencia, CA, USA) and mixed with RT² SYBR Green Mastermix (QIAGEN, Valencia, CA, USA) before aliquoting in a 96-well RT² Profiler PCR Array for human apoptosis (PAHS-012Z, QIAGEN, Valencia, CA, USA). In total, 84 key genes involved in the apoptosis pathway were included, where 52, 24, and 8 were classified as pro-apoptotic, apoptosis-related, and anti-apoptotic genes, respectively, classified according to the manufacturer and the Gene Ontology (GO) database.

The cycle threshold (Ct) values obtained were converted to Δ Ct values based on the gene of interest versus the geometric mean of the housekeeping genes (*ACTB*, *B2M*, *GAPDH*, *HPRT1*, and *RPLP0*). Thereafter, the mean relative $\Delta\Delta$ Ct was calculated for each treatment in relation to the mean Δ Ct of the vehicle control group. By implementing the $2^{-\Delta\Delta$ Ct method, treated vs. control, we obtained a fold change (FC) value for each gene [33]. Genes were defined as differentially expressed if $|FC| > 1.5$.

2.6. Statistical Analyses

All calculations and statistical analyses were made with GraphPad Prism version 9.4.1.681 (GraphPad Software, Boston, MA, USA) and Excel 2013 for Windows (Microsoft Corporation, Redmond, WA, USA). The relative tumor volume (RTV) was determined individually for each mouse and time point, and mean value and the standard error of the mean (SEM) were calculated for each group. One-way ANOVA was used for estimating the statistical differences regarding tumor volume between all groups throughout the treatment period. The Student's *t*-test was applied for comparison between groups. $p < 0.05$ was considered statistically significant different.

A theoretical value of the level of additive effect of both monotherapies (¹⁷⁷Lu-octreotide and lorlatinib, respectively) was calculated based on The Bliss independence model, assuming an independent effect of each monotherapy [34,35]. Firstly, the fractional response, *F*, of each monotherapy was estimated in relation to vehicle control.

$$F_{\text{monotherapy}} = 1 - \frac{RTV_{\text{monotherapy}}}{RTV_{\text{control}}} \quad (2)$$

Subsequently, the theoretical additive effect was estimated.

$$F_{\text{additive}} = F_{\text{Lorlatinib}} + F_{^{177}\text{Lu-octreotide}} - F_{\text{Lorlatinib}} \times F_{^{177}\text{Lu-octreotide}} \quad (3)$$

The theoretical additive effect value was calculated for days 4 to 14 and illustrated as a dashed line in Figure 1C for each time point. An effect of combination therapy larger than the theoretical additive effect (lower F_{additive}) was regarded as synergistic, and if the effect was smaller (higher F_{additive}) it was regarded as antagonistic.

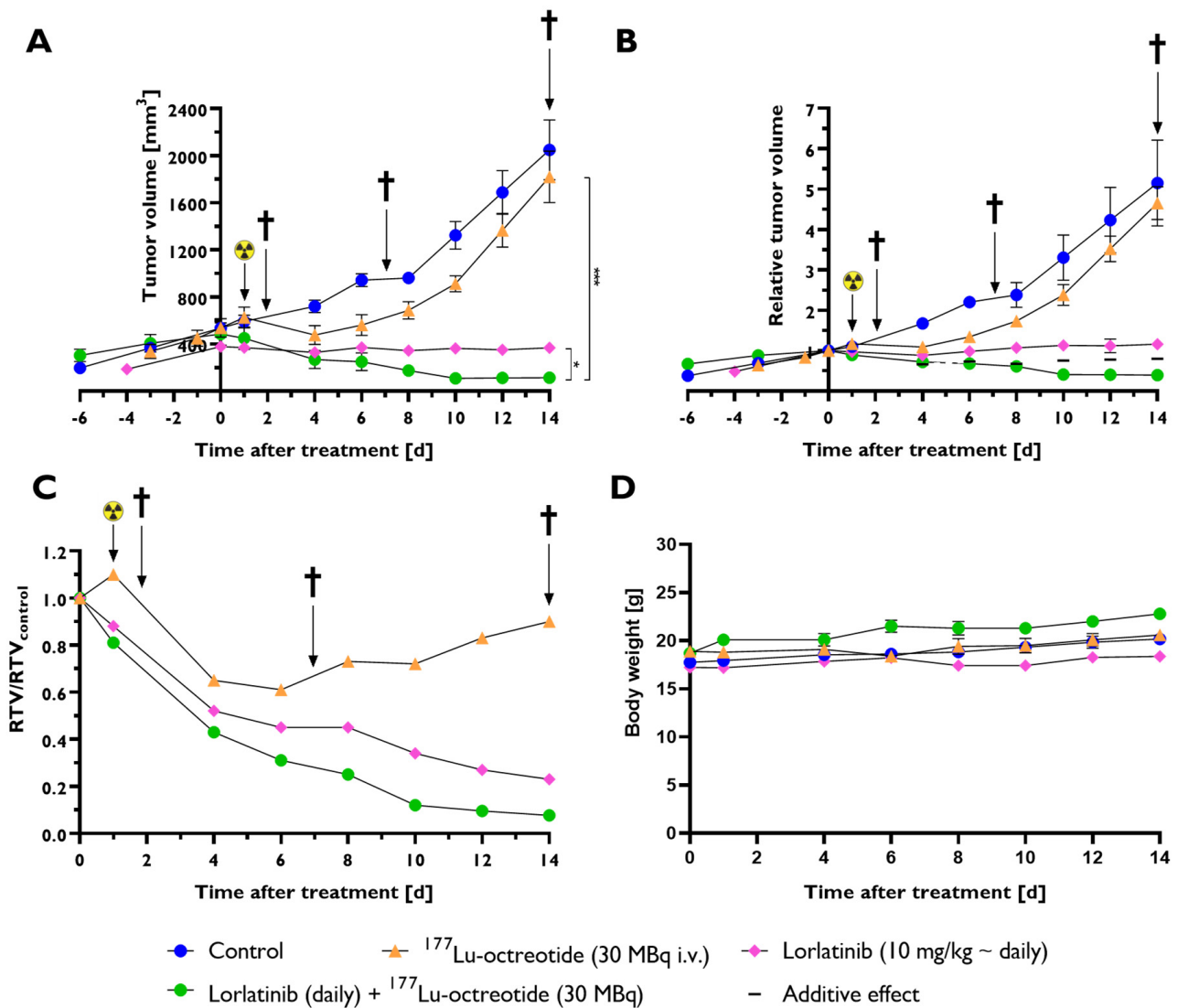


Figure 1. Effect of treatment with either lorlatinib (pink), ¹⁷⁷Lu-octreotide (orange) or both in combination (green) in mice bearing human CLB-BAR NB xenografts on tumor volume (A–C) and body weight (D). Mice were treated with lorlatinib (daily gavage, 10 mg/kg), and/or ¹⁷⁷Lu-octreotide (30 MBq i.v. on day 1, symbolized by the radiation symbol) or i.v. injected with saline on day 1 (control) ($n = 10$ mice/group on day 0). The effect of each monotherapy and the combination therapy is shown as mean tumor volume (mm³) (A) and relative tumor volume (RTV) (B). A theoretical additive effect was calculated using the Bliss independence model (Bliss C. 1939) and presented as a dashed line in (B). (C) The RTV-ratio (RTV/RTV_{control}) for all treated groups is shown. Three mice from each group were sacrificed (†) on day 2 and day 7, respectively, and the remaining four mice in each group were sacrificed on day 14. Whole body weight of each group is presented in (D). Error bars represent SEM, not always visible because of their low values, * indicates $p < 0.05$ and *** $p < 0.0001$.

For mRNA expression analyses, Student's *t*-tests were applied to compare Δ Ct-values of deregulated genes post treatment with vehicle control. $p < 0.05$ was considered statistically significant.

For immunohistochemical analyses, a Jarque–Bera test for normality showed that the Histoscores for CC3 staining did not have a normal distribution (p -value < 0.001), possibly due to the low number of samples. Because of this, the non-parametric Kruskal–Wallis test with Dunn's Multiple Comparison Test was used to compare differences between groups.

3. Results

3.1. Combination Therapy Gave the Largest Tumor Volume Reduction

BALB/c nude mice with sc CLB-BAR NB xenografts were treated with either lorlatinib, ¹⁷⁷Lu-octreotide, or both in combination over 14 days. Combined therapy with both lorlatinib and ¹⁷⁷Lu-octreotide yielded the greatest antitumor effect with a RTV of 0.39 at day 14 (Figure 1A,B). The corresponding RTV value at day 14 for lorlatinib monotherapy was 1.2. ¹⁷⁷Lu-octreotide as monotherapy (i.v. injection at day 1) demonstrated an initial decrease in RTV compared to control, with the lowest RTV of 1.1 on day 4, after which RTV increased to 4.6 on day 14 and displayed a similar tumor growth as the control group from day 8 to 14. RTV decreased between days 1 and 4 by 7.1%, 9.8%, and 19% for ¹⁷⁷Lu-octreotide monotherapy, lorlatinib monotherapy, and combination therapy, respectively. The RTV in the controls increased monotonically reaching 5.2 on day 14. Combination therapy showed a more prominent antitumor effect than the theoretical value of the additive effect of both monotherapies combined from day 6 (Figure 1B).

To further illustrate the differences between each treatment versus control, we calculated the RTV ratio ($RTV_{\text{therapy}}/RTV_{\text{control}}$ (RTV-ratio) over the 14 day treatment (Figure 1C). ¹⁷⁷Lu-octreotide monotherapy resulted in a decrease in RTV ratio on day 4 that continued until day 6 and then gradually increased. In contrast, the RTV ratios of the lorlatinib and combination treatment groups decreased throughout the treatment period and reached 0.23 and 0.08 on day 14, respectively. One-way ANOVA demonstrated a significant difference between all groups from day 4 to 14, with $p < 0.001$ at all studied time points. No significant weight loss was observed in any group (Figure 1D).

3.2. Changes in the Expression of Genes Involved in Apoptosis

To better understand the effect of treatment on CLB-BAR xenograft growth, we harvested tumors at days 2, 7, and 14 of treatment and performed qPCR analyses for 84 selected genes, including pro-apoptotic genes (Figure 2) and anti-apoptotic and apoptosis-related genes (Figure 3). Lorlatinib treatment resulted in mRNA expression changes in 5 of the 79 detected transcripts from the 84 gene panel ($|FC| > 1.5$). In response to lorlatinib, all significantly regulated genes were down-regulated, two genes (*TNFRSF9* and *BIRC3*) were found after 7 days, and four genes (*CASP8*, *CD40*, *BIRC3*, and *BNIP3L*) were found 14 days post treatment. Three pro-apoptotic genes were down-regulated in comparison with the control: *CASP8*, *CD40*, and *TNFRSF9* (Figure 2). *BIRC3*, categorized as anti-apoptotic, was down-regulated after 7 and 14 days (Figure 3). *BNIP3L*, categorized as apoptosis related, was down-regulated after 14 days (Figure 3).

Treatment with ¹⁷⁷Lu-octreotide yielded expression changes in 9 unique genes of 79 detectable mRNAs (Figures 2 and 3). Six of the genes were classified as pro-apoptotic: *BCL2AI*, *CASPI*, *FASLG*, *TNFRSF10A*, *TNFRSF1B*, and *TNFSF8*. *BCL2AI*, *CASPI*, *FASLG*, and *TNFSF8* (day 14) were down-regulated, whereas *TNFRSF10A*, *TNFRSF1B*, and *TNFSF8* (day 7) were up-regulated (Figure 2). Two of the genes were classified as anti-apoptotic, *BCL2L10* and *CD40LG*, detected as down- and up-regulated, respectively. *TP73*, classified as apoptosis related, was found to be down-regulated.

Combination treatment with both lorlatinib and ¹⁷⁷Lu-octreotide resulted in differential expression of 23 unique genes of 78 detectable mRNAs (Figures 2 and 3). In total, 13 pro-apoptotic genes, namely, *BCL2LII*, *BID*, *CASP5*, *CASP8*, *CASP9*, *FAS*, *FASLG*, *GADD45A*, *HRK*, *LTA*, *LTBR*, *TNFRSF10A*, and *TNFRSF1B*, exhibited differences in expression (Figure 2); only *BID* and *CASP8* were down-regulated, while the remaining genes were up-regulated. *CASP9* was up-regulated at both 2 and 7 days (Figure 2). Seven anti-apoptotic genes, namely, *BCL2LI0*, *BCL2L2*, *BIRC3*, *CD40LG*, *CIDEA*, *IL10*, and *NOL3*, were differentially expressed. Of these genes, *IL10* was the only down-regulated gene, and the remaining genes were up-regulated (Figure 3). *CD40LG* was commonly found to be up-regulated after 2 and 7 days (Figure 3). Three apoptosis-related genes, namely, *BNIP3*, *BNIP3L*, and *TNF*, were down-regulated.

Lorlatinib			¹⁷⁷ Lu-octreotide			Lorlatinib + ¹⁷⁷ Lu-octreotide			Gene
2d	7d	14d	2d	7d	14d	2d	7d	14d	
FC (-/+)	FC (-/+)	FC (-/+)	FC (-/+)	FC (-/+)	FC (-/+)	FC (-/+)	FC (-/+)	FC (-/+)	
-0.13	0.08	-0.13	-0.17	0.02	-0.02	-0.32	0.01	-0.03	ABL1
-0.29	-0.56	-0.12	-0.28	-0.03	0.63	-0.50	-0.23	0.10	AIFM1
-0.26	-0.14	-0.43	0.12	0.10	0.16	0.91	0.19	0.04	APAF1
0.12	0.18	0.11	0.23	0.95	0.50	1.08	0.17	0.84	BAD
0.19	0.21	0.15	0.24	0.12	-0.11	-0.22	-0.11	0.40	BAK1
0.06	-0.15	-0.23	0.87	0.82	0.37	0.88	0.21	0.29	BAX
					-1.62				BCL2A1
0.42	-0.20	-0.56	0.49	0.57	-0.22	1.81	0.78	-0.31	BCL2L1
0.11	0.26	0.60	-0.28	-0.24	-0.10	-1.62	-0.63	-0.14	BID
0.41	0.82	0.07	0.49	0.90	0.38	1.32	0.49	0.76	BIK
0.67	0.11	0.17	0.27	0.25	0.45	1.20	0.97	0.98	BRAF
			-1.82		-0.26			1.13	CASP1
-0.16	-1.26	-0.95	0.14	0.72	-0.99	-0.17	0.83	-0.27	CASP10
									CASP14
0.01	0.15	0.01	0.07	0.25	0.09	-0.40	-0.62	0.28	CASP2
-0.39	0.34	0.67	-0.11	0.39	0.71	-0.95	-0.12	0.75	CASP3
-0.87	-0.96	-0.05	-0.20	-0.04	0.08	-0.48	-0.89	-0.01	CASP4
							2.22		CASP5
-0.21	-0.17	-1.15	0.16	0.80	0.38	-0.21	-0.08	-0.74	CASP6
0.02	-0.36	-0.39	0.20	0.08	0.43	0.07	-0.73	-0.71	CASP7
-0.43	-0.86	-1.62	-0.14	0.33	-0.63	-0.54	-0.46	-1.78	CASP8
0.04	-0.25	-0.05	-0.18	0.71	-0.10	1.83	1.96	-0.17	CASP9
-0.80	-1.47	-2.34	0.11	1.16	-0.31	0.72	0.73	-1.22	CD40
0.04	0.15	0.28	0.03	0.29	0.05	-0.34	-0.21	0.63	CIDEB
0.32	0.35	-0.52	0.54	-0.24	-0.53	-0.23	-0.70	-0.84	CRADD
0.22	0.28	0.16	0.44	0.91	-0.26	0.15	-0.09	0.57	CYCS
0.99	0.74	0.56	0.78	1.15	0.85	0.41	0.35	1.06	DAPK1
0.04	0.01	0.43	-0.01	-0.10	0.14	-0.33	-0.35	0.47	DFFA
0.00	0.12	-0.08	-0.31	0.08	-0.20	-0.05	-0.20	0.24	DIABLO
0.03	0.56	0.43	-0.47	0.28	0.25	-0.04	-0.26	0.08	FADD
0.06	-0.64	-0.50	0.96	0.80	-0.11	1.83	1.01	0.72	FAS
-0.43	0.25	0.84	0.88	0.31	-1.60	1.79	1.37	0.29	FASLG
-0.63	-0.26	-1.00	0.03	0.09	-0.32	2.04	-0.18	-0.40	GADD45A
0.19	-0.04	-0.66	-0.13	0.95	1.13	3.35	3.02	0.80	HRK
	1.48	-0.88	-1.24	1.41	-1.07		3.04	-0.03	LTA
		-0.56		0.91	-0.61		4.78		LTBR
-0.04	-0.19	-0.28	-0.05	0.20	0.08	-0.45	-0.33	0.32	NOD1
0.16	1.00	0.88	0.15	1.27	0.70	0.77	1.11	1.46	PYCARD
-0.26	-0.30	-0.37	-0.14	0.08	0.09	0.11	-0.14	-0.08	RIPK2
0.09	-0.87	-1.29	1.91	1.36	-0.20	2.75	1.15	-0.61	TNFRSF10A
-0.46	-0.82	-1.23	0.68	0.41	-0.03	1.23	-0.46	-0.33	TNFRSF10B
									TNFRSF11B
-0.01	0.47	-0.29	0.21	1.12	0.32	1.18	0.34	0.75	TNFRSF1A
0.56	1.03	-1.06	1.12	2.43	-1.11	2.10	1.46	0.20	TNFRSF1B
-0.09	-0.05	0.12	-0.35	0.50	0.41	-1.01	-0.09	0.40	TNFRSF21
	-1.52	0.26		0.27	0.65				TNFRSF9
0.11	0.03	-0.47	0.71	0.52	-1.19	1.42	1.22	-0.34	TNFSF10
0.40	0.71	0.14	0.67	1.70	-1.64				TNFSF8
-0.09	-0.19	-0.32	-0.32	-0.04	-0.03	-0.19	-0.21	-0.21	TP53BP2
									TRADD
-0.12	0.41	0.50	0.12	0.56	0.52	-0.11	-0.26	0.73	TRAF2
0.27	-0.16	0.23	0.44	0.49	0.62	0.57	-0.27	0.99	TRAF3

Pro-apoptotic genes

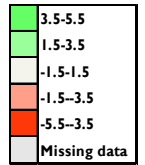
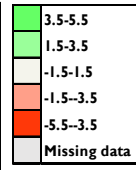


Figure 2. mRNA expression of 52 pro-apoptotic genes in tumor tissue (CLB-BAR) from mice treated with lorlatinib and/or ¹⁷⁷Lu-octreotide, expressed as fold change (FC) relative to controls. Tumors were analyzed from mice sacrificed on day 2 (*n* = 3), day 7 (*n* = 3), or day 14 (*n* = 4). Red and green colors represent down- and up-regulation, respectively, with |FC| > 1.5. Missing data are represented by gray color.

Lorlatinib			¹⁷⁷ Lu-octreotide			Lorlatinib + ¹⁷⁷ Lu-octreotide			Gene
2d	7d	14d	2d	7d	14d	2d	7d	14d	
FC (-/+)	FC (-/+)	FC (-/+)	FC (-/+)	FC (-/+)	FC (-/+)	FC (-/+)	FC (-/+)	FC (-/+)	
0.02	0.60	0.79	0.25	0.37	0.49	-0.42	0.59	0.60	BAG1
-0.16	-0.22	0.03	0.17	0.00	-0.08	0.77	-0.56	-0.62	BAG3
0.64	0.36	0.08	0.76	1.36	0.79	1.19	1.48	0.99	BCL2
0.08	0.14	-0.20	0.20	0.71	0.19	0.29	0.07	0.42	BCL2L1
	-0.56	-0.02	-1.71	-1.34	-0.53		1.63	0.98	BCL2L10
0.18	-0.16	0.35	-0.01	0.16	0.51	1.52	-0.04	0.59	BCL2L2
-0.19	-0.09	-0.05	-0.17	0.05	0.12	-0.33	-0.45	-0.17	BFAR
-0.20	-0.51	-0.68	-0.20	0.07	0.14	0.23	-0.24	-0.60	BIRC2
0.19	-1.67	-2.08	0.25	0.63	0.19	2.90	0.38	-0.50	BIRC3
-0.34	0.37	0.21	0.51	0.43	0.63	-0.63	0.36	1.02	BIRC5
-0.02	-0.04	0.25	-0.02	0.27	0.37	0.21	0.07	0.50	BIRC6
0.09	-0.10	-0.27	0.21	0.54	0.23	0.87	0.06	0.38	BNIP2
0.14	1.47	-0.26	0.94	3.36	-1.22	2.56	4.14	0.22	CD40LG
0.04		-0.17			-0.43			0.23	CD70
0.38	-0.08	-0.33	0.49	0.80	0.27	1.01	0.47	0.16	CFLAR
0.88	0.10	-0.49	1.45	0.99	-0.62	2.25	0.83	0.38	CIDEA
0.68	0.77	0.55	0.01	0.35	0.12	1.27	0.90	0.65	IGF1R
	-1.20	-0.90		0.72			-1.92		IL10
-0.17	0.04	0.56	0.25	0.22	0.21	-0.34	-0.02	0.92	MCL1
0.12	0.24	0.40	-0.40	-0.39	0.14	-0.14	0.52	0.39	NAIP
-0.06	0.06	0.02	0.01	0.02	0.26	-0.09	-0.24	0.44	NFKB1
0.83	0.53	0.92	0.18	0.62	0.37	1.07	0.46	1.64	NOL3
-0.29	0.10	-0.35	-0.20	0.79	0.38	1.35	0.86	0.25	TNFRSF25
0.15	0.45	0.39	-0.42	-0.17	0.05	-0.52	-0.16	-0.18	XIAP
0.04	-0.16	0.16	0.01	0.42	0.40	-0.16	-0.63	0.60	AKT1
0.13	-0.02	-0.23	0.07	0.49	0.19	0.85	0.37	0.31	BCL10
						4.58			BNIP3
-0.37	-0.93	-1.71	0.09	0.31	0.17	2.58	0.01	-1.38	BNIP3L
0.53	0.77	0.41	-0.08	0.14	-0.71	0.30	0.87	-0.10	CD27
				0.51		4.78			TNF
-0.37	-0.41	-1.08	-0.08	0.24	-0.08	-0.62	-1.17	-0.97	TP53
0.99	0.29	0.02	1.36	1.02	-1.55		-0.78	-0.56	TP73



Anti-apoptotic genes

Apoptosis related

Figure 3. mRNA expression of 24 anti-apoptotic and 8 apoptosis related genes in tumor tissue (CLB-BAR) from mice treated with lorlatinib and/or ¹⁷⁷Lu-octreotide, expressed as fold change (FC) relative to controls. Tumors analyzed were from mice sacrificed on day 2 (*n* = 3), day 7 (*n* = 3) or day 14 (*n* = 4). Red and green colors represent down- and up-regulation, respectively, with |FC| > 1.5. Missing data are represented by gray color.

Figure 4 illustrates the overall transcriptional response for the statistically significant regulated genes (|FC| > 1.5, *p* < 0.05). The presented genes are relevant in both intrinsic (*BID*, *BNIP3L*, *CASP9*, and *HRK*) and extrinsic (*CASP8*, *CD40*, *FASLG*, *NOL3*, and *TNFRSF10A*) apoptosis pathways. At 2 and 7 days after treatment started, the majority of significantly regulated genes were found in the combination group, and most of them were pro-apoptotic. Most of the genes were also up-regulated compared with the control group. This pattern was not observed at 14 d.

3.3. Immunohistochemical Analyses

We next analyzed apoptosis at the protein level in treated tumors employing antibodies against cleaved caspase 3 (CC3). Immunohistochemical examination identified CC3-positive cells (with nuclear staining) at days 2 and 14 after treatment start (Figure 5). Overall, we observed an increase in CC3-positive cells (Histoscore) in tumors from treated mice, with the exception of lorlatinib on day 2, with the highest Histoscore for combination-

treated tumors on day 2. However, there was a large spread within the groups, and statistical significance was only observed at day 14 in the combination group.

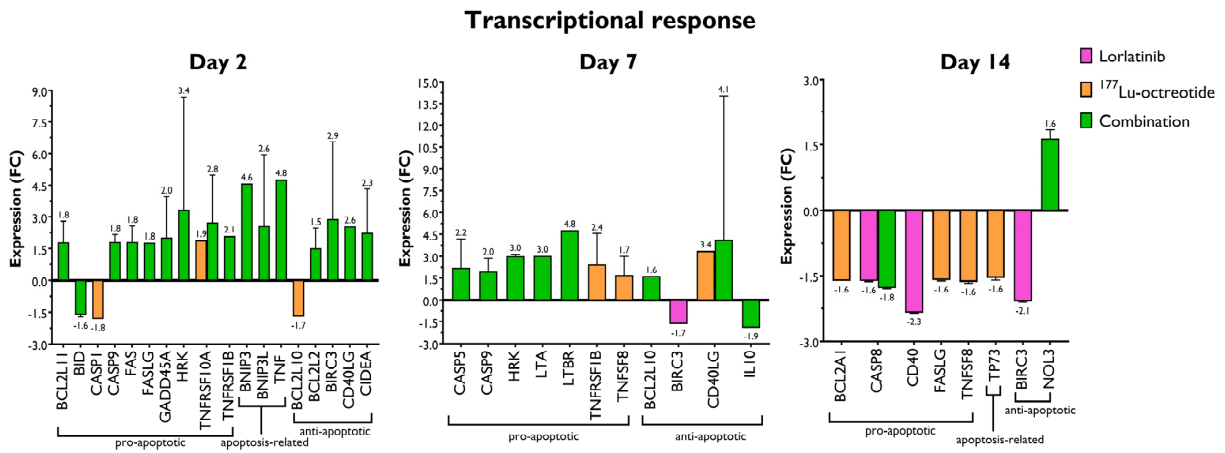


Figure 4. mRNA expression of pro-apoptotic, anti-apoptotic, and apoptosis-related genes in human NB xenograft tumor tissue (CLB-BAR) from mice treated with lorlatinib and/or ¹⁷⁷Lu-octreotide, expressed as fold change (FC) relative to controls, on day 2 (n = 3), day 7 (n = 3) or day 14 (n = 4). Only differentially regulated genes with |FC| > 1.5 are presented. Error bars indicate SEM.

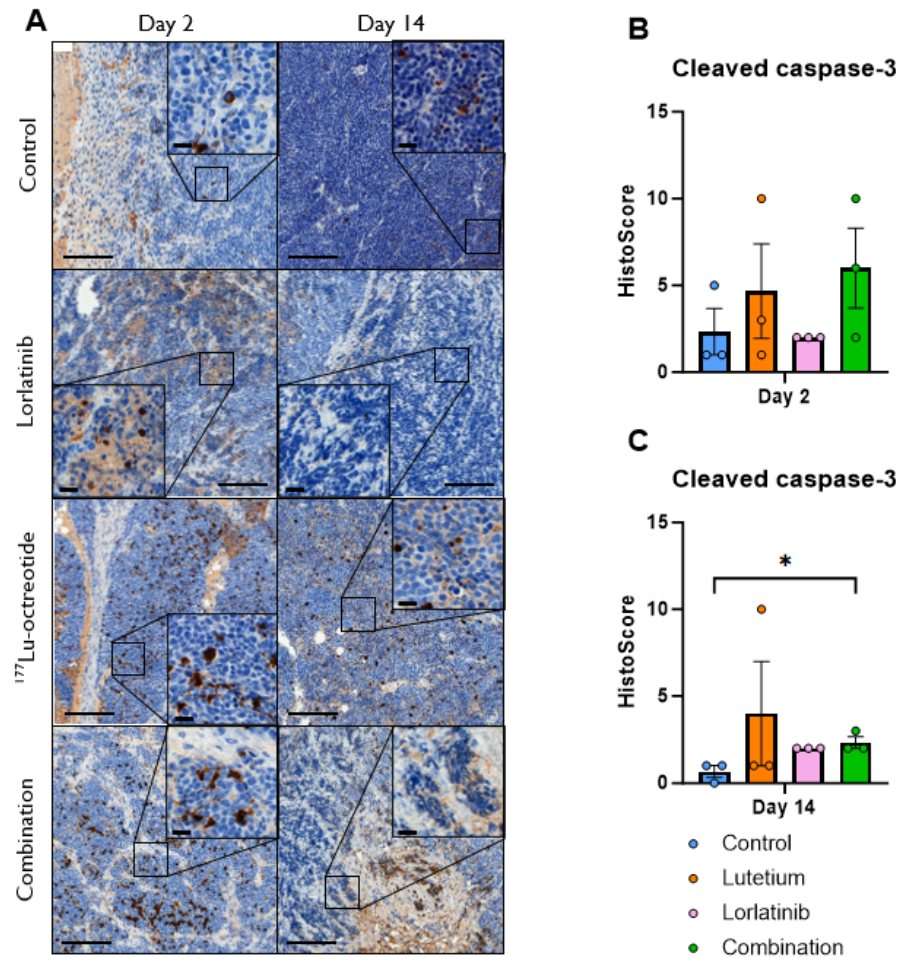


Figure 5. (A) Immunohistochemical staining for cleaved caspase-3 (CC3) in CLB-BAR tumors, 2 and 14 days post treatment. Lorlatinib was administered daily via oral gavage from day 0, ¹⁷⁷Lu-octreotide

was administered i.v. on day 1 in both the combination group and the monotherapy and the control were i.v. injected with saline on day 1. Numerous CC3-positive cells (brown color) were found in all images (counterstained with hematoxylin), with the highest intensity (visually) in the treated groups. Scale bars equals 200 μm and 20 μm (40 \times magnified inserts). (B,C) Distribution of CC3 HistoScore in CLB-BAR tumors at 2 (B) and 14 days (C) after treatment start for controls (blue), ^{177}Lu -octreotide (orange), lorlatinib (pink), and both ^{177}Lu -octreotide and lorlatinib in combination (green). The mean HistoScore value was calculated for each group based on the intensity (graded: 0, negative; 1, weak; 2, moderate; or 3, strong) and the percentage of positive cells. Error bars represent SEM. * represents $p < 0.05$ calculated using Kruskal–Wallis test with Dunn’s Multiple Comparison Test.

4. Discussion

Lorlatinib, a third-generation ALK inhibitor, has emerged as a treatment alternative for ALK-positive HR-NB [13]. Lorlatinib demonstrates enhanced activity and efficiency against ALK mutations compared to previous generations of ALKi [10–12]. Nevertheless, several studies have reported lorlatinib resistance in response to treatment, emphasizing the need for a multimodal therapy approach [15–18]. Systemic treatment with radiolabeled SSTAs, e.g., ^{177}Lu -octreotide, is successfully used for SSTR-overexpressing neuroendocrine tumors. To our knowledge, this is the first study examining and reporting radio-sensitization and synergistic antitumor effects in an ALK-amplified and SSTR-positive HR-NB xenograft model with lorlatinib and ^{177}Lu -octreotide.

The present study was performed on CLB-BAR cells with *MYCN* amplification and ALK gain-of-function that may represent high-risk neuroblastomas [32,36]. In the mice, the CLB-BAR tumor volume reduction was moderate after treatment with ^{177}Lu -octreotide, which is consistent with results from a previous study in the same animal model, comparing effects of ^{177}Lu -octreotide and ^{177}Lu -octreotate [37]. Although biodistribution and biokinetics were most favorable for ^{177}Lu -octreotate, resulting in higher absorbed dose to tumor for ^{177}Lu -octreotate, the tumor volume reduction was somewhat better for ^{177}Lu -octreotide.

It should be noted that we purposefully employed low doses of ^{177}Lu -octreotide and lorlatinib in this study to enable visualization of additive or synergistic effects. The administered amounts were based on previous work using CLB-BAR xenografts [12,37–39], and while higher doses of each drug have been tested without significant adverse effects, the combination of drugs with different mechanisms of action might result in different or enhanced toxicities. This further warrants the choice of lower administered amounts in this study. The moderate therapeutic effects of ^{177}Lu -octreotide monotherapy despite high uptake and retention in NB compared with other neuroendocrine tumors in similar models are unexpected, since the therapeutic effects in such studies were much more dramatic, with a possibility to eradicate the tumor totally [40–43]. CLB-BAR has a high proliferation rate and tumor growth curve compared with other neuroendocrine tumor models of, e.g., intestinal origin, which might influence the therapeutic response [42]. Monotherapy with lorlatinib resulted in a cytostatic response. Thus, the present results are difficult to interpret, and may be related to certain properties in NB. Detailed signaling pathway analyses will be needed in order to understand the radioresistance in NB, and contribute to a better understanding, needed for future optimization of therapy with radiolabeled SSTAs. It is, however, clear that inhibition of ALK with lorlatinib may act to overcome some of the radioresistance in CLB-BAR NB cell xenografts.

ALK signals via several downstream pathways, having a considerable role in, e.g., cell cycle progression, survival, DNA repair, proliferation, and angiogenesis, via Ras-extracellular signal-regulated kinase (Erk), PI3K-AKT-mTOR and Janus protein tyrosine kinase (JAK)-STAT [38,44,45]. However, how these signaling pathways are affected by irradiation, either alone or in combination with an ALKi, has not been explored. The present study demonstrated that treatment of CLB-BAR tumors with lorlatinib in combination with ^{177}Lu -octreotide synergistically reduced tumor volume and resulted in elevated transcription of genes involved in apoptosis. Several studies suggest that inhibiting critical mediators of the DNA damage response (DDR) can enhance radiosensitivity [45–49]. Dol-

man et al. demonstrated radiosensitization of NB cells by inhibiting the DNA-dependent protein kinase catalytic subunit (DNA-PKcs), playing a central role in the repair of DNA double-strand breaks (DSBs) via non-homologous end-joining (NHEJ) [46]. Further, a combination of ^{177}Lu -octreotate and a p53 stabilizing drug showed better therapeutic effects compared to monotherapy in NB cell spheroids and NB xenografts on mice [50,51]. Altogether, these findings indicate a possible role for DNA repair inhibition in the enhanced response to ^{177}Lu -octreotide combined with lorlatinib. Previous studies have illustrated the radiosensitizing effects of crizotinib, the first generation of ALKi, in combination with external radiation in ALK-positive non-small cell lung cancer (NSCLC) models [52,53]. The Akt kinase is one common mediator in both DDR and ALK pathways [54,55]. DNA damage sensors, e.g., DNA-PKcs, phosphorylate Akt in the DDR pathway due to, e.g., radiation-induced DSBs [54]. Subsequently, phosphorylated Akt promotes NHEJ-mediated DSB repair and cell survival [54]. Hence, elevated levels of phosphorylated Akt is associated with malignant tumors and poor prognosis [56,57]. Lorlatinib can, like crizotinib, aggravate NHEJ-mediated DSB repair by partially inhibiting Akt, a downstream signaling effector of ALK, and act as a radiosensitizer. However, a driving force in lorlatinib resistance for HR-NB is the activation of bypass pathways, such as EGFR, ErbB4, and RAS [15,58]. Other reported mechanisms causing ALKi-resistance are structural alterations in the kinase domain, leading to a decreased binding of ALKi, as well as amplification of *ALK* [59]. Identifying the specific mechanisms underlying the drug-resistant properties that arise in response to ALKi treatments is essential for further treatment. In several patient case reports where relapse has occurred, multiple biopsies distributed throughout the treatment have been employed to modify the choice of ALKi to provide an optimal treatment strategy [60–63]. Of special interest is a case where an ALK-positive NSCLC gained resensitization to crizotinib after acquiring resistance to lorlatinib, highlighting the critical information provided via biopsies and the remarkable mechanisms behind ALKi resistance [64].

Given the well-documented heterogeneous properties of NB [65], it may be necessary to eradicate tumor cells via various targets, aiming to eradicate multiple sub-populations of tumor cells and thus eliminate resistance. Based on our results, radiolabeled SSTAs may be a beneficial adjunctive treatment for disseminated SSTR-positive HR-NBs. Pilot trials with ^{177}Lu -octreotate, an alternative SSTA, have shown varied results for NB patients, highlighting the need for optimization according to each patient's specific tumor characteristics [27–29]. In addition, to avoid under-treatment, the biokinetics of the radiopharmaceutical need to be investigated before the start of the treatment. In the ongoing phase II trial with HR-NB patients, LuDO-N, ^{68}Ga -octreotide PET/CT examination will be used to determine activity levels of the two ^{177}Lu -octreotate administrations, not exceeding mean absorbed dose levels to the organs at risk (23 and 2.4 Gy to kidneys and whole body, respectively) [30]. Combining this information with information regarding eventual gain-of-function *ALK* mutations to, if possible, determine an appropriate ALKi for combination therapy is a further step to individualize the treatment.

The transcriptional response of the 84 genes involved in apoptosis provided another demonstration of the synergistic antitumor effect provided by the combination therapy. In total, 40 genes were up- or down-regulated, with the strongest differential gene expression observed in the ^{177}Lu -octreotide/lorlatinib combination therapy arm in which 26 genes were modulated, compared with 10 in response to ^{177}Lu -octreotide treatment, and only 4 with lorlatinib. Overall, a higher number of pro-apoptotic genes were up-regulated in the combination therapy at earlier time points, although more anti-apoptotic genes were also up-regulated at the same time. After statistical analysis of the ΔCt values (treated vs. control), only the combination treatment yielded a significant effect on the transcriptional response of genes within the Bcl-2 family (Table 1). Proteins of the Bcl-2 family are essential for apoptotic cell death in health and disease through different mechanisms [66–69]. Functionally categorized as pro-apoptotic or anti-apoptotic proteins within the Bcl-2 family, the imbalance of concentrations leads to cell survival or death [66,67].

Conversely, the tumor cells can continue their growth and progress if apoptosis can be inhibited, meaning that increased levels of anti-apoptotic proteins are associated with oncogenesis [67]. Our data demonstrated down-regulation of *BID* (BH3-interacting domain death agonist) on day 2, and up-regulation of *HRK* (Harakiri, BCL2 interacting protein) on day 7, both classified as pro-apoptotic genes. *BID* encodes for a protein (Bid) that connects the extrinsic apoptotic pathway with the intrinsic [70]. Cleaved Bid is translocated to the mitochondria and induces cytochrome c release, subsequently promoting downstream caspase activation [70]. Hrk is a BH3-only protein, encoded by *HRK*, and regulates apoptosis by displacing Bim or Bid from anti-apoptotic Bcl-xL, also leading to cytochrome c release and caspase activation [67,71]. The relatively strong up-regulation of *HRK* (fold change 3.02) suggests a possible mechanism for the increased apoptosis observed in Figure 5. Future studies should investigate the involvement of Bcl-xL in resistance to ALK inhibitors or radiolabeled SSTAs, and the potential use of BCL2-family inhibitors in combination with these modalities.

Table 1. Functional characterization of differentially regulated genes after treatment with either lorlatinib, ¹⁷⁷Lu-octreotide, or both in combination. Differential gene expression is expressed as fold change (FC) relative to control. Only genes exhibiting $|FC| > 1.5$ and $p < 0.05$ are presented. Lilac, yellow, and brown colors represent classification as pro-apoptotic, apoptosis-related, and anti-apoptotic genes, respectively.

Gene	Description	Protein Family	FC	<i>p</i>	Time after Treatment, Treatment
CASP8	Caspase 8, apoptosis-related cysteine peptidase	Caspase family	−1.62	0.0003	14 days, Lorlatinib
CD40	CD40 molecule, TNF receptor superfamily member 5	TNF-receptor superfamily	−2.34	0.0001	14 days, Lorlatinib
BNIP3L	BCL2/adenovirus interacting protein 3-like	Pro-apoptotic subfamily within the Bcl-2 family	−1.71	0.0001	14 days, Lorlatinib
BIRC3	Baculoviral IAP repeat containing 3	Inhibition of apoptosis (IAP) family	−1.67 −2.08	0.0218 0.0005	7 days, Lorlatinib 14 days, Lorlatinib
FASLG	Fas ligand (TNF superfamily, member 6)	TNF superfamily	−1.60	0.0036	14 days, ¹⁷⁷ Lu-octreotide
TNFRSF10A	TNF receptor superfamily, member 10a	TNF-receptor superfamily	1.91	0.0004	2 days, ¹⁷⁷ Lu-octreotide
TP73	Tumor protein p73	TP53 family	−1.55	0.0380	14 days, ¹⁷⁷ Lu-octreotide
BID	BH3 interacting domain death agonist	Bcl-2 family	−1.62	0.0356	2 days, Combination
CASP8	Caspase 8, apoptosis-related cysteine peptidase	Caspase family	−1.78	0.0003	14 days, Combination
CASP9	Caspase 9, apoptosis-related cysteine peptidase	Caspase family	1.83 1.96	0.0011 0.0103	2 days, Combination 7 days, Combination
HRK	Harakiri, BCL2 interacting protein (contains only BH3 domain)	Bcl-2 family	3.02	0.0014	7 days, Combination
TNFRSF10A	TNF receptor superfamily, member 10a	TNF-receptor superfamily	2.75	0.0254	2 days, Combination
NOL3	Nucleolar protein 3 (apoptosis repressor with CARD domain)	Down-regulates activities of caspase 2, 8 and p53	1.64	0.0011	14 days, Combination

Other genes with their associated protein families belonged to caspase, tumor necrosis factor (TNF), and p53. The caspase family executes cell death via a cascade of activations. Various members are involved in both the extrinsic and intrinsic apoptotic pathways,

and are classified as initiator or effector caspases [67,72]. *CASP8*, encoding the initiator caspase-8 (extrinsic pathway), was down-regulated on day 14 post treatment with lorlatinib and the combination. Conversely, *CASP9*, encoding for the initiator caspase-9 (intrinsic pathway), was up-regulated for the combination on days 2 and 7. TNF and TNF-receptor (TNFR) superfamilies are involved in the extrinsic signaling pathway of apoptosis and are activated by ligand binding to receptors [73]. Within the TNFR superfamily, *TNFRSF10A* was up-regulated on day 2 for both ¹⁷⁷Lu-octreotide and the combination. Whereas *CD40* was down-regulated on day 14 for lorlatinib, *FASLG*, encoding for Fas ligand belonging to the TNF superfamily, was down-regulated on day 14 for ¹⁷⁷Lu-octreotide. The tumor-suppressor family p53 is one of the most frequently mutated genes in cancer [74,75]; within this family, *TP73* was down-regulated on day 14 for ¹⁷⁷Lu-octreotide. TP73 is involved in the regulation of, i.e., tissue development and inflammation [74,76].

The number of genes with larger spread (larger error bars) in mRNA expression were more prominent early after exposure (day 2, i.e., 1 day after injection with ¹⁷⁷Lu-octreotide), with only a few at day 7 and none at day 14. High SEM values were in general due to one or two very high values, all values in the same regulation direction. Most of these genes were differentially expressed in the group given the combination therapy. There may be several reasons for different expression between tumors in different mice: the relatively low doses given that may result in various effects, the early time point when differences in signaling is more probable, and the heterogeneous nature of NB.

Compared with two previous studies in a human small-intestine NET GOT1 mouse model where the transcriptional response was studied after treatment with ¹⁷⁷Lu-octreotate, some genes are commonly found. For example, *BNIP3L* (apoptosis-related) was up-regulated 41 days after administration with 15 MBq ¹⁷⁷Lu-octreotate. However, in the present study, *BNIP3L* was down-regulated after lorlatinib treatment on days 7 and 14 [77]. Besides comparing different tumor types, the relatively large time difference between the GOT1 and the present study may suggest that the tumors were in different phases after treatment, tumor regrowth vs. tumor shrinkage, and explain differences in the transcriptional response. In another study on the GOT1 model, *BIRC3* (anti-apoptotic) was up-regulated one day post administration with 30 MBq ¹⁷⁷Lu-octreotate [78], whereas it was down-regulated after lorlatinib treatment on days 7 and 14. A common up-regulation of the death receptor genes *TNFRSF10A* and *TNFRSF10B*, was also observed. *TNFRSF10A* was up-regulated on day 2 after the combination treatment (present study), while *TNFRSF10B* was up-regulated on days 1 and 7 post treatment with 30 MBq ¹⁷⁷Lu-octreotate in the GOT1 study.

We complemented our gene expression analyses with immunohistochemistry for CC3 to study apoptosis at the protein level, as caspase 3 has a central role in both apoptotic pathways as an executioner caspase. CC3 positivity was increased in response to treatment with the exception of lorlatinib on both day 2 and day 14. The presence of cleaved caspase 3 in cells is a clear indication of a cell undergoing apoptosis. However, since this process results in dismantling of the cellular components and eventual phagocytosis by, e.g., macrophages, the timing of the cleaved caspase 3 expression and staining positivity can be difficult, especially considering that ¹⁷⁷Lu-octreotide is retained in the tumor cells resulting in prolonged irradiation of the cell. This means that the expression of cleaved caspase 3 will not occur simultaneously in all treated cells, and the expression will not last over a long period of time since the dying cells are removed continuously. This results in higher variability in the staining for cleaved caspase 3. However, the changes were large enough to be statistically significant in the combination group on day 14.

In future studies, it would be interesting to combine fractionated/repeated administration of ¹⁷⁷Lu-octreotide in combination with lorlatinib. In a previous study in the same animal model, we observed that fractionated administration of ¹⁷⁷Lu-octreotate with short intervals resulted in a more prominent antitumor effect due to higher uptake in tumor cells because of recycling of SSTRs counteracting the likely SSTR saturation effects that prevail with a single injection of higher amounts of SSTAs [37].

Treatment of HR-NB poses a challenge since most cases are diagnosed as an advanced, metastasized, and, therefore, inoperable disease. Although an intense treatment approach has been successful for certain patients, it is not always obvious which patients benefit most from them. And as the patient group is children, intensive treatments are avoided as much as possible because of the late effects. Hence, a multimodal approach could benefit two aspects: increased tumor control and mitigating side effects. Our study highlights the radiosensitizing nature of lorlatinib in NB-bearing mice. The fact that both treatments are systemic enables their combination in cases where the cancer has metastasized. Today, both lorlatinib and radiolabeled SSTAs are being studied separately in various phase I/II trials for HR-NBs, enabling the course for a possible combination for the cases where the prerequisites are met [14,30].

5. Conclusions

Synergistic antitumor effects were found when lorlatinib and ^{177}Lu -octreotide treatment was combined in an HR-NB xenograft mouse model. Combination therapy also had a more significant impact on expression of genes involved in apoptotic processes, for example up-regulation of the Bcl-xL inhibitor *HRK*. This was shown to result in a significant increase in cleaved caspase 3 in tumor cells receiving combination therapy. The data suggest that inhibiting ALK signaling plays a role in the radiosensitization of radionuclide therapy with ^{177}Lu -octreotide, implying a potential for clinical application of combining ALKi with radiolabeled SSTAs for HR-NBs overexpressing SSTRs and ALK.

Author Contributions: A.R., B.H., R.H.P., J.S., K.H. and E.F.-A. designed and conceptualized the study; D.E.L. and D.P. carried out the cell culturing; D.P. and A.R. conducted the animal experiments; H.B. and A.R. were responsible for the labeling of ^{177}Lu . A.R., K.S. and N.R. contributed to the RNA extraction and the validation steps involved; K.S. and A.R. were responsible for the qPCR and the following data measurements; A.R., E.F.-A., N.R. and J.S. contributed to the data analysis and interpretations. All authors reviewed and edited the manuscript. All authors have read and agreed to the published version of the manuscript.

Funding: This study was supported by grants from the Swedish Research Council (EFA: 2021-02636; RHP: 2019-03914; BH: 2021-01192), the Swedish Cancer Society (EFA: CAN20/1293 and 23 2975; RHP: CAN21/1459; BH: CAN21/1525), Swedish Childhood Cancer Foundation (EFA: PR2017-0057; RHP: PR2022-0029; BH: PR2021-0027), BioCARE—a National Strategic Research Program at University of Gothenburg, the Swedish state under the agreement between the Swedish government and the county councils—the ALF-agreement (ALFGBG-966074), the King Gustav V Jubilee Clinic Cancer Research Foundation, the Sahlgrenska University Hospital Research Funds, Wilhelm and Martina Lundgren Research Foundation, Assar Gabrielsson Cancer Research Foundation, Herbert & Karin Jacobsson Foundation, and Adlerbertska Research Foundation.

Institutional Review Board Statement: The study was conducted according to the guidelines of the Declaration of Helsinki, and approved by the Swedish Ethical Committee on Animal Experiments in Gothenburg (protocol code 2779-20 and date of approval 2020-08-26).

Informed Consent Statement: Not applicable.

Data Availability Statement: The original contributions presented in the study are included in the article, further inquiries can be directed to the corresponding author.

Conflicts of Interest: The authors declare no conflict of interest.

References

1. Umopathy, G.; Mendoza-Garcia, P.; Hallberg, B.; Palmer, R.H. Targeting anaplastic lymphoma kinase in neuroblastoma. *APMIS* **2019**, *127*, 288–302. [[CrossRef](#)]
2. De Brouwer, S.; De Preter, K.; Kumps, C.; Zabrocki, P.; Porcu, M.; Westerhout, E.M.; Lakeman, A.; Vandesompele, J.; Hoebeeck, J.; Van Maerken, T.; et al. Meta-analysis of neuroblastomas reveals a skewed ALK mutation spectrum in tumors with MYCN amplification. *Clin. Cancer Res.* **2010**, *16*, 4353–4362. [[CrossRef](#)] [[PubMed](#)]

3. Eleveld, T.F.; Oldridge, D.A.; Bernard, V.; Koster, J.; Daage, L.C.; Diskin, S.J.; Schild, L.; Bentahar, N.B.; Bellini, A.; Chicard, M.; et al. Relapsed neuroblastomas show frequent RAS-MAPK pathway mutations. *Nat. Genet.* **2015**, *47*, 864–871. [[CrossRef](#)] [[PubMed](#)]
4. Pugh, T.J.; Morozova, O.; Attiyeh, E.F.; Asgharzadeh, S.; Wei, J.S.; Auclair, D.; Carter, S.L.; Cibulskis, K.; Hanna, M.; Kiezun, A.; et al. The genetic landscape of high-risk neuroblastoma. *Nat. Genet.* **2013**, *45*, 279–284. [[CrossRef](#)]
5. Berry, T.; Luther, W.; Bhatnagar, N.; Jamin, Y.; Poon, E.; Sanda, T.; Pei, D.; Sharma, B.; Vetharoy, W.R.; Hallsworth, A.; et al. The ALKF1174L mutation potentiates the oncogenic activity of MYCN in neuroblastoma. *Cancer Cell* **2012**, *22*, 117–130. [[CrossRef](#)]
6. Zhu, S.; Lee, J.S.; Guo, F.; Shin, J.; Perez-Atayde, A.R.; Kutok, J.L.; Rodig, S.J.; Neuberg, D.S.; Helman, D.; Feng, H.; et al. Activated ALK collaborates with MYCN in neuroblastoma pathogenesis. *Cancer Cell* **2012**, *21*, 362–373. [[CrossRef](#)]
7. Schönherr, C.; Ruuth, K.; Kamaraj, S.; Wang, C.-L.; Yang, H.-L.; Combaret, V.; Djos, A.; Martinsson, T.; Christensen, J.G.; Palmer, R.H.; et al. Anaplastic Lymphoma Kinase (ALK) regulates initiation of transcription of MYCN in neuroblastoma cells. *Oncogene* **2012**, *31*, 5193–5200. [[CrossRef](#)]
8. Morgenstern, D.A.; Bagatell, R.; Cohn, S.L.; Hogarty, M.D.; Maris, J.M.; Moreno, L.; Park, J.R.; Pearson, A.D.; Schleiermacher, G.; Valteau-Couanet, D.; et al. The challenge of defining “ultra-high-risk” neuroblastoma. *Pediatr. Blood Cancer* **2019**, *66*, e27556. [[CrossRef](#)] [[PubMed](#)]
9. Johnson, T.W.; Richardson, P.F.; Bailey, S.; Brooun, A.; Burke, B.J.; Collins, M.R.; Cui, J.J.; Deal, J.G.; Deng, Y.-L.; Dinh, D.; et al. Discovery of (10 R)-7-Amino-12-fluoro-2, 10, 16-trimethyl-15-oxo-10, 15, 16, 17-tetrahydro-2H-8, 4-(metheno) pyrazolo [4, 3-h][2, 5, 11]-benzoxadiazacyclotetradecine-3-carbonitrile (PF-06463922), a macrocyclic inhibitor of anaplastic lymphoma kinase (ALK) and c-ros oncogene 1 (ROS1) with preclinical brain exposure and broad-spectrum potency against ALK-resistant mutations. *J. Med. Chem.* **2014**, *57*, 4720–4744.
10. Syed, Y.Y. Lorlatinib: First global approval. *Drugs* **2019**, *79*, 93–98. [[CrossRef](#)]
11. Zou, H.Y.; Friboulet, L.; Kodack, D.P.; Engstrom, L.D.; Li, Q.; West, M.; Tang, R.W.; Wang, H.; Tsaparikos, K.; Wang, J.; et al. PF-06463922, an ALK/ROS1 inhibitor, overcomes resistance to first and second generation ALK inhibitors in preclinical models. *Cancer Cell* **2015**, *28*, 70–81. [[CrossRef](#)] [[PubMed](#)]
12. Guan, J.; Tucker, E.R.; Wan, H.; Chand, D.; Danielson, L.S.; Ruuth, K.; El Wakil, A.; Witek, B.; Jamin, Y.; Umapathy, G.; et al. The ALK inhibitor PF-06463922 is effective as a single agent in neuroblastoma driven by expression of ALK and MYCN. *Dis. Models Mech.* **2016**, *9*, 941–952. [[CrossRef](#)] [[PubMed](#)]
13. Liu, T.; Merguerian, M.D.; Rowe, S.P.; Pratilas, C.A.; Chen, A.R.; Ladle, B.H. Exceptional response to the ALK and ROS1 inhibitor lorlatinib and subsequent mechanism of resistance in relapsed ALK F1174L-mutated neuroblastoma. *Mol. Case Stud.* **2021**, *7*, a006064. [[CrossRef](#)] [[PubMed](#)]
14. Goldsmith, K.C.; Park, J.R.; Kayser, K.; Malvar, J.; Chi, Y.-Y.; Groshen, S.G.; Villablanca, J.G.; Krytska, K.; Lai, L.M.; Acharya, P.T.; et al. Lorlatinib with or without chemotherapy in ALK-driven refractory/relapsed neuroblastoma: Phase 1 trial results. *Nat. Med.* **2023**, *29*, 1092–1102. [[CrossRef](#)] [[PubMed](#)]
15. Redaelli, S.; Ceccon, M.; Zappa, M.; Sharma, G.G.; Mastini, C.; Mauri, M.; Nigoghossian, M.; Massimino, L.; Cordani, N.; Farina, F.; et al. Lorlatinib Treatment Elicits Multiple On- and Off-Target Mechanisms of Resistance in ALK-Driven Cancer. *Cancer Res.* **2018**, *78*, 6866–6880. [[CrossRef](#)] [[PubMed](#)]
16. Mizuta, H.; Okada, K.; Araki, M.; Adachi, J.; Takemoto, A.; Kutkowska, J.; Maruyama, K.; Yanagitani, N.; Oh-Hara, T.; Watanabe, K.; et al. Gilteritinib overcomes lorlatinib resistance in ALK-rearranged cancer. *Nat. Commun.* **2021**, *12*, 1261. [[CrossRef](#)] [[PubMed](#)]
17. Okada, K.; Araki, M.; Sakashita, T.; Ma, B.; Kanada, R.; Yanagitani, N.; Horiike, A.; Koike, S.; Oh-Hara, T.; Watanabe, K.; et al. Prediction of ALK mutations mediating ALK-TKIs resistance and drug re-purposing to overcome the resistance. *EBioMedicine* **2019**, *41*, 105–119. [[CrossRef](#)] [[PubMed](#)]
18. Xie, B.; Qiu, Y.; Zhou, J.; Du, D.; Ma, H.; Ji, J.; Zhu, L.; Zhang, W. Establishment of an acquired lorlatinib-resistant cell line of non-small cell lung cancer and its mediated resistance mechanism. *Clin. Transl. Oncol.* **2022**, *24*, 2231–2240. [[CrossRef](#)] [[PubMed](#)]
19. Lamberts, S.W.; Krenning, E.P.; Reubi, J.C. The Role of Somatostatin and Its Analogs in the Diagnosis and Treatment of Tumors. *Endocr. Rev.* **1991**, *12*, 450–482. [[CrossRef](#)]
20. Baum, R.P.; Kluge, A.W.; Kulkarni, H.; Schorr-Neufing, U.; Niepsch, K.; Bitterlich, N.; van Echteld, C.J. [¹⁷⁷Lu-DOTA] 0-D-Phe1-Tyr3-octreotide (¹⁷⁷Lu-DOTATOC) for peptide receptor radiotherapy in patients with advanced neuroendocrine tumours: A phase-II study. *Theranostics* **2016**, *6*, 501. [[CrossRef](#)]
21. Esser, J.P.; Krenning, E.P.; Teunissen, J.J.M.; Kooij, P.P.M.; Van Gameren, A.L.H.; Bakker, W.H.; Kwekkeboom, D.J. Comparison of [¹⁷⁷Lu-DOTA0, Tyr3] octreotate and [¹⁷⁷Lu-DOTA0, Tyr3] octreotide: Which peptide is preferable for PRRT? *Eur. J. Nucl. Med. Mol. Imaging* **2006**, *33*, 1346–1351. [[CrossRef](#)]
22. Reubi, J.C.; Schär, J.-C.; Waser, B.; Wenger, S.; Heppeler, A.; Schmitt, J.S.; Mäcke, H.R. Affinity profiles for human somatostatin receptor subtypes SST1–SST5 of somatostatin radiotracers selected for scintigraphic and radiotherapeutic use. *Eur. J. Nucl. Med.* **2000**, *27*, 273–282. [[CrossRef](#)]
23. Uusijärvi, H.; Bernhardt, P.; Ericsson, T.; Forsell-Aronsson, E. Dosimetric characterization of radionuclides for systemic tumor therapy: Influence of particle range, photon emission, and subcellular distribution. *Med. Phys.* **2006**, *33*, 3260–3269. [[CrossRef](#)]
24. Uusijärvi, H.; Bernhardt, P.; Rösch, F.; Maecke, H.R.; Forsell-Aronsson, E. Electron- and positron-emitting radiolanthanides for therapy: Aspects of dosimetry and production. *J. Nucl. Med.* **2006**, *47*, 807–814. [[PubMed](#)]

25. Swärd, C.; Bernhardt, P.; Ahlman, H.; Wängberg, B.; Forssell-Aronsson, E.; Larsson, M.; Svensson, J.; Rossi-Norrlund, R.; Kölby, L. [¹⁷⁷Lu-DOTA0-Tyr3]-octreotate treatment in patients with disseminated gastroenteropancreatic neuroendocrine tumors: The value of measuring absorbed dose to the kidney. *World J. Surg.* **2010**, *34*, 1368–1372. [[CrossRef](#)] [[PubMed](#)]
26. Romiani, A.; Spetz, J.; Shubbar, E.; Lind, D.E.; Hallberg, B.; Palmer, R.H.; Forssell-Aronsson, E. Neuroblastoma xenograft models demonstrate the therapeutic potential of ¹⁷⁷Lu-octreotate. *BMC Cancer* **2021**, *21*, 950. [[CrossRef](#)]
27. Gains, J.E.; Bomanji, J.B.; Fersht, N.L.; Sullivan, T.; D'Souza, D.; Sullivan, K.P.; Aldridge, M.; Waddington, W.; Gaze, M.N. ¹⁷⁷Lu-DOTATATE molecular radiotherapy for childhood neuroblastoma. *J. Nucl. Med.* **2011**, *52*, 1041–1047. [[CrossRef](#)] [[PubMed](#)]
28. Kong, G.; Hofman, M.S.; Murray, W.K.; Wilson, S.; Wood, P.; Downie, P.; Super, L.; Hogg, A.; Eu, P.; Hicks, R.J. Initial experience with gallium-68 DOTA-octreotate PET/CT and peptide receptor radionuclide therapy for pediatric patients with refractory metastatic neuroblastoma. *J. Pediatr. Hematol. Oncol.* **2016**, *38*, 87–96. [[CrossRef](#)]
29. Gains, J.E.; Moroz, V.; Aldridge, M.D.; Wan, S.; Wheatley, K.; Laidler, J.; Peet, C.; Bomanji, J.B.; Gaze, M.N. A phase IIa trial of molecular radiotherapy with ¹⁷⁷-lutetium DOTATATE in children with primary refractory or relapsed high-risk neuroblastoma. *Eur. J. Nucl. Med. Mol. Imaging* **2020**, *47*, 2348–2357. [[CrossRef](#)]
30. Sundquist, F.; Georgantzi, K.; Jarvis, K.B.; Brok, J.; Koskenvuo, M.; Rascon, J.; van Noesel, M.; Grybäck, P.; Nilsson, J.; Braat, A.; et al. A Phase II Trial of a Personalized, Dose-Intense Administration Schedule of ¹⁷⁷Lutetium-DOTATATE in Children With Primary Refractory or Relapsed High-Risk Neuroblastoma—LuDO-N. *Front. Pediatr.* **2022**, *10*, 167. [[CrossRef](#)]
31. Forssell-Aronsson, E.; Spetz, J.; Ahlman, H. Radionuclide therapy via SSTR: Future aspects from experimental animal studies. *Neuroendocrinology* **2013**, *97*, 86–98. [[CrossRef](#)] [[PubMed](#)]
32. Fransson, S.; Hansson, M.; Ruuth, K.; Djos, A.; Berbegall, A.; Javanmardi, N.; Abrahamsson, J.; Palmer, R.H.; Noguera, R.; Hallberg, B.; et al. Intragenic anaplastic lymphoma kinase (ALK) rearrangements: Translocations as a novel mechanism of ALK activation in neuroblastoma tumors. *Genes Chromosomes Cancer* **2015**, *54*, 99–109. [[CrossRef](#)] [[PubMed](#)]
33. Schmittgen, T.D.; Livak, K.J. Analyzing real-time PCR data by the comparative CT method. *Nat. Protoc.* **2008**, *3*, 1101–1108. [[CrossRef](#)] [[PubMed](#)]
34. Bliss, C.I. The toxicity of poisons applied jointly 1. *Ann. Appl. Biol.* **1939**, *26*, 585–615. [[CrossRef](#)]
35. Sandblom, V.; Spetz, J.; Shubbar, E.; Montelius, M.; Ståhl, I.; Swanpalmer, J.; Nilsson, O.; Forssell-Aronsson, E. Gemcitabine potentiates the anti-tumour effect of radiation on medullary thyroid cancer. *PLoS ONE* **2019**, *14*, e0225260. [[CrossRef](#)] [[PubMed](#)]
36. Cazes, A.; Louis-Brennetot, C.; Mazot, P.; Dingli, F.; Lombard, B.; Boeva, V.; Daveau, R.; Cappo, J.; Combaret, V.; Schleiermacher, G.; et al. Characterization of Rearrangements Involving the ALK Gene Reveals a Novel Truncated Form Associated with Tumor Aggressiveness in Neuroblastoma. *Cancer Res.* **2013**, *73*, 195–204. [[CrossRef](#)] [[PubMed](#)]
37. Romiani, A.; Simonsson, K.; Pettersson, D.; Al-Awar, A.; Rassol, N.; Bakr, H.; Lind, D.E.; Umaphathy, G.; Spetz, J.; Palmer, R.H.; et al. Comparison of ¹⁷⁷Lu-octreotate and ¹⁷⁷Lu-octreotide for treatment in human neuroblastoma-bearing mice. *Heliyon* **2024**, *10*, e31409. [[CrossRef](#)] [[PubMed](#)]
38. Szydzik, J.; Lind, D.E.; Arefin, B.; Kurhe, Y.; Umaphathy, G.; Siaw, J.T.; Claeys, A.; Gabre, J.L.; Eynden, J.V.D.; Hallberg, B.; et al. ATR inhibition enables complete tumour regression in ALK-driven NB mouse models. *Nat. Commun.* **2021**, *12*, 6813. [[CrossRef](#)] [[PubMed](#)]
39. Romiani, A. Improved Radionuclide Therapy of Neuroblastoma—Preclinical Evaluation of ¹⁷⁷Lu-Labeled Somatostatin Analogs. Ph.D. Thesis, University of Gothenburg, Gothenburg, Sweden, 2023.
40. Kölby, L.; Bernhardt, P.; Johanson, V.; Schmitt, A.; Ahlman, H.; Forssell-Aronsson, E.; Mäcke, H.; Nilsson, O. Successful receptor-mediated radiation therapy of xenografted human midgut carcinoid tumour. *Br. J. Cancer* **2005**, *93*, 1144–1151. [[CrossRef](#)]
41. Swärd, C.; Bernhardt, P.; Johanson, V.; Schmitt, A.; Ahlman, H.; Stridsberg, M.; Forssell-Aronsson, E.; Nilsson, O.; Kölby, L. Comparison of [¹⁷⁷Lu-DOTA0, Tyr3]-octreotate and [¹⁷⁷Lu-DOTA0, Tyr3]-octreotide for receptor-mediated radiation therapy of the xenografted human midgut carcinoid tumor GOT1. *Cancer Biother. Radiopharm.* **2008**, *23*, 114–120. [[CrossRef](#)]
42. Elvborn, M.; Shubbar, E.; Forssell-Aronsson, E. Hyperfractionated Treatment with ¹⁷⁷Lu-Octreotate Increases Tumor Response in Human Small-Intestine Neuroendocrine GOT1 Tumor Model. *Cancers* **2022**, *14*, 235. [[CrossRef](#)] [[PubMed](#)]
43. Schmitt, A.; Bernhardt, P.; Nilsson, O.; Ahlman, H.; Kölby, L.; Forssell-Aronsson, E. Differences in biodistribution between ^{99m}Tc-depreotide, ¹¹¹In-DTPA-octreotide, and ¹⁷⁷Lu-DOTA-Tyr3-octreotate in a small cell lung cancer animal model. *Cancer Biother. Radiopharm.* **2005**, *20*, 231–236. [[CrossRef](#)] [[PubMed](#)]
44. Ducray, S.P.; Natarajan, K.; Garland, G.D.; Turner, S.D.; Egger, G. The transcriptional roles of ALK fusion proteins in tumorigenesis. *Cancers* **2019**, *11*, 1074. [[CrossRef](#)] [[PubMed](#)]
45. Borenäs, M.; Umaphathy, G.; Lind, D.E.; Lai, W.-Y.; Guan, J.; Johansson, J.; Jennische, E.; Schmidt, A.; Kurhe, Y.; Gabre, J.L.; et al. ALK signaling primes the DNA damage response sensitizing ALK-driven neuroblastoma to therapeutic ATR inhibition. *Proc. Natl. Acad. Sci. USA* **2024**, *121*, e2315242121. [[CrossRef](#)]
46. Dolman, M.E.M.; van der Ploeg, I.; Koster, J.; Bate-Eya, L.T.; Versteeg, R.; Caron, H.N.; Molenaar, J.J. DNA-dependent protein kinase as molecular target for radiosensitization of neuroblastoma cells. *PLoS ONE* **2015**, *10*, e0145744. [[CrossRef](#)] [[PubMed](#)]
47. Toulany, M.; Kehlback, R.; Florczak, U.; Sak, A.; Wang, S.; Chen, J.; Loblrich, M.; Rodemann, H.P. Targeting of AKT1 enhances radiation toxicity of human tumor cells by inhibiting DNA-PKcs-dependent DNA double-strand break repair. *Mol. Cancer Ther.* **2008**, *7*, 1772–1781. [[CrossRef](#)] [[PubMed](#)]
48. Stronach, E.A.; Chen, M.; Maginn, E.N.; Agarwal, R.; Mills, G.B.; Wasan, H.; Gabra, H. DNA-PK mediates AKT activation and apoptosis inhibition in clinically acquired platinum resistance. *Neoplasia* **2011**, *13*, 1069–IN35. [[CrossRef](#)]

49. Dong, J.; Ren, Y.; Zhang, T.; Wang, Z.; Ling, C.C.; Li, G.C.; He, F.; Wang, C.; Wen, B. Inactivation of DNA-PK by knockdown DNA-PKcs or NU7441 impairs non-homologous end-joining of radiation-induced double strand break repair. *Oncol. Rep.* **2018**, *39*, 912–920. [[CrossRef](#)]
50. Lundsten, S.; Berglund, H.; Jha, P.; Krona, C.; Hariri, M.; Nelander, S.; Lane, D.P.; Nestor, M. p53-Mediated Radiosensitization of (¹⁷⁷)Lu-DOTATATE in Neuroblastoma Tumor Spheroids. *Biomolecules* **2021**, *11*, 1695. [[CrossRef](#)]
51. Berglund, H.; Salomonsson, S.L.; Mohajershojai, T.; Gago, F.J.F.; Lane, D.P.; Nestor, M. p53 stabilisation potentiates [(¹⁷⁷)Lu]Lu-DOTATATE treatment in neuroblastoma xenografts. *Eur. J. Nucl. Med. Mol. Imaging* **2024**, *51*, 768–778. [[CrossRef](#)]
52. Sun, Y.; Nowak, K.A.; Zaorsky, N.G.; Winchester, C.L.; Dalal, K.; Giacalone, N.J.; Liu, N.; Werner-Wasik, M.; Wasik, M.A.; Dicker, A.P.; et al. ALK Inhibitor PF02341066 (Crizotinib) Increases Sensitivity to Radiation in Non-Small Cell Lung Cancer Expressing EML4-ALKPF02341066 Sensitizes EML4-ALK NSCLC Cells to Radiation Treatment. *Mol. Cancer Ther.* **2013**, *12*, 696–704. [[CrossRef](#)] [[PubMed](#)]
53. Dai, Y.; Wei, Q.; Schwager, C.; Moustafa, M.; Zhou, C.; Lipson, K.E.; Weichert, W.; Debus, J.; Abdollahi, A. Synergistic effects of crizotinib and radiotherapy in experimental EML4-ALK fusion positive lung cancer. *Radiother. Oncol.* **2015**, *114*, 173–181. [[CrossRef](#)] [[PubMed](#)]
54. Liu, Q.; Turner, K.M.; Alfred Yung, W.K.; Chen, K.; Zhang, W. Role of AKT signaling in DNA repair and clinical response to cancer therapy. *Neuro-Oncol.* **2014**, *16*, 1313–1323. [[CrossRef](#)] [[PubMed](#)]
55. Iida, M.; Harari, P.M.; Wheeler, D.L.; Toulany, M. Targeting AKT/PKB to improve treatment outcomes for solid tumors. *Mutat. Res.* **2020**, *819*, 111690. [[CrossRef](#)] [[PubMed](#)]
56. Zheng, H.; Zhang, Y.; Liu, S.; Lu, J.; Yang, Y.; Wen, Q.; Fan, S. Elevated expression of G3BP1 associates with YB1 and p-AKT and predicts poor prognosis in nonsmall cell lung cancer patients after surgical resection. *Cancer Med.* **2019**, *8*, 6894–6903. [[CrossRef](#)] [[PubMed](#)]
57. Opel, D.; Poremba, C.; Simon, T.; Debatin, K.M.; Fulda, S. Activation of Akt predicts poor outcome in neuroblastoma. *Cancer Res.* **2007**, *67*, 735–745. [[CrossRef](#)] [[PubMed](#)]
58. Berlak, M.; Tucker, E.; Dorel, M.; Winkler, A.; McGearey, A.; Rodriguez-Fos, E.; da Costa, B.M.; Barker, K.; Fyle, E.; Calton, E.; et al. Mutations in ALK signaling pathways conferring resistance to ALK inhibitor treatment lead to collateral vulnerabilities in neuroblastoma cells. *Mol. Cancer* **2022**, *21*, 126. [[CrossRef](#)] [[PubMed](#)]
59. Lin, J.J.; Riely, G.J.; Shaw, A.T. Targeting ALK: Precision Medicine Takes on Drug Resistance. *Cancer Discov.* **2017**, *7*, 137–155. [[CrossRef](#)] [[PubMed](#)]
60. Makuuchi, Y.; Hayashi, H.; Haratani, K.; Tanizaki, J.; Tanaka, K.; Takeda, M.; Sakai, K.; Shimizu, S.; Ito, A.; Nishio, K.; et al. A case of ALK-rearranged non-small cell lung cancer that responded to ceritinib after development of resistance to alectinib. *Oncotarget* **2018**, *9*, 23315. [[CrossRef](#)] [[PubMed](#)]
61. Sharma, G.G.; Cortinovis, D.; Agustoni, F.; Arosio, G.; Villa, M.; Cordani, N.; Bidoli, P.; Bisson, W.H.; Pagni, F.; Piazza, R.; et al. A compound L1196M/G1202R ALK mutation in a patient with ALK-positive lung cancer with acquired resistance to brigatinib also confers primary resistance to lorlatinib. *J. Thorac. Oncol.* **2019**, *14*, e257–e259. [[CrossRef](#)]
62. Takahashi, K.; Seto, Y.; Okada, K.; Uematsu, S.; Uchibori, K.; Tsukahara, M.; Oh-Hara, T.; Fujita, N.; Yanagitani, N.; Nishio, M.; et al. Overcoming resistance by ALK compound mutation (I1171S + G1269A) after sequential treatment of multiple ALK inhibitors in non-small cell lung cancer. *Thorac. Cancer* **2020**, *11*, 581–587. [[CrossRef](#)]
63. Recondo, G.; Mezquita, L.; Facchinetti, F.; Planchard, D.; Gazzah, A.; Bigot, L.; Rizvi, A.Z.; Frias, R.L.; Thiery, J.P.; Scoazec, J.Y.; et al. Diverse Resistance Mechanisms to the Third-Generation ALK Inhibitor Lorlatinib in ALK-Rearranged Lung Cancer Resistance to Lorlatinib in ALK-Rearranged Lung Cancer. *Clin. Cancer Res.* **2020**, *26*, 242–255. [[CrossRef](#)] [[PubMed](#)]
64. Shaw, A.T.; Friboulet, L.; Leshchiner, I.; Gainor, J.F.; Bergqvist, S.; Brooun, A.; Burke, B.J.; Deng, Y.L.; Liu, W.; Dardaei, L.; et al. Resensitization to crizotinib by the lorlatinib ALK resistance mutation L1198F. *New Engl. J. Med.* **2016**, *374*, 54–61. [[CrossRef](#)]
65. Gomez, R.L.; Ibragimova, S.; Ramachandran, R.; Philpott, A.; Ali, F.R. Tumoral heterogeneity in neuroblastoma. *Biochim. Biophys. Acta Rev. Cancer* **2022**, *1877*, 188805. [[CrossRef](#)]
66. Youle, R.J.; Strasser, A. The BCL-2 protein family: Opposing activities that mediate cell death. *Nat. Rev. Mol. Cell Biol.* **2008**, *9*, 47–59. [[CrossRef](#)]
67. Singh, R.; Letai, A.; Sarosiek, K. Regulation of apoptosis in health and disease: The balancing act of BCL-2 family proteins. *Nat. Rev. Mol. Cell Biol.* **2019**, *20*, 175–193. [[CrossRef](#)] [[PubMed](#)]
68. Spetz, J.K.E.; Florido, M.H.C.; Fraser, C.S.; Qin, X.; Choiniere, J.; Yu, S.J.; Singh, R.; Friesen, M.; Rubin, L.L.; Salem, J.-E.; et al. Heightened apoptotic priming of vascular cells across tissues and life span predisposes them to cancer therapy-induced toxicities. *Sci. Adv.* **2022**, *8*, eabn6579. [[CrossRef](#)]
69. Singh, R.; Yu, S.; Osman, M.; Inde, Z.; Fraser, C.; Cleveland, A.H.; Almanzar, N.; Lim, C.B.; Joshi, G.N.; Spetz, J.; et al. Radiotherapy-Induced Neurocognitive Impairment Is Driven by Heightened Apoptotic Priming in Early Life and Prevented by Blocking BAX. *Cancer Res.* **2023**, *83*, 3442–3461. [[CrossRef](#)] [[PubMed](#)]
70. Yin, X.-M. Signal transduction mediated by Bid, a pro-death Bcl-2 family proteins, connects the death receptor and mitochondria apoptosis pathways. *Cell Res.* **2000**, *10*, 161–167. [[CrossRef](#)]
71. Kaya-Aksoy, E.; Cingoz, A.; Senbabaoglu, F.; Seker, F.; Sur-Erdem, I.; Kayabolen, A.; Lokumcu, T.; Sahin, G.N.; Karahuseyinoglu, S.; Bagci-Onder, T. The pro-apoptotic Bcl-2 family member Harakiri (HRK) induces cell death in glioblastoma multiforme. *Cell Death Discov.* **2019**, *5*, 64. [[CrossRef](#)]

72. Fan, T.J.; Han, L.H.; Cong, R.S.; Liang, J. Caspase family proteases and apoptosis. *Acta Biochim. Et Biophys. Sin.* **2005**, *37*, 719–727. [[CrossRef](#)] [[PubMed](#)]
73. Dostert, C.; Grusdat, M.; Letellier, E.; Brenner, D. The TNF family of ligands and receptors: Communication modules in the immune system and beyond. *Physiol. Rev.* **2019**, *99*, 115–160. [[CrossRef](#)] [[PubMed](#)]
74. Morris, S.M. A role for p53 in the frequency and mechanism of mutation. *Mutat. Res./Rev. Mutat. Res.* **2002**, *511*, 45–62. [[CrossRef](#)] [[PubMed](#)]
75. Marei, H.E.; Althani, A.; Afifi, N.; Hasan, A.; Caceci, T.; Pozzoli, G.; Morriore, A.; Giordano, A.; Cenciarelli, C. p53 signaling in cancer progression and therapy. *Cancer Cell Int.* **2021**, *21*, 703. [[CrossRef](#)] [[PubMed](#)]
76. Zawacka-Pankau, J.E. The Role of p53 Family in Cancer. *Cancers* **2022**, *14*, 823. [[CrossRef](#)] [[PubMed](#)]
77. Spetz, J.; Rudqvist, N.; Langen, B.; Parris, T.Z.; Dalmo, J.; Schöler, E.; Wängberg, B.; Nilsson, O.; Helou, K.; Forssell-Aronsson, E. Time-dependent transcriptional response of GOT1 human small intestine neuroendocrine tumor after ¹⁷⁷Lu [Lu]-octreotate therapy. *Nucl. Med. Biol.* **2018**, *60*, 11–18. [[CrossRef](#)]
78. Rassol, N.; Andersson, C.; Pettersson, D.; Al-Awar, A.; Shubbar, E.; Kovács, A.; Åkerström, B.; Gram, M.; Helou, K.; Forssell-Aronsson, E. Co-administration with AIM does not influence apoptotic response of (¹⁷⁷)Lu-octreotate in GOT1 neuroendocrine tumors. *Sci. Rep.* **2023**, *13*, 6417. [[CrossRef](#)]

Disclaimer/Publisher’s Note: The statements, opinions and data contained in all publications are solely those of the individual author(s) and contributor(s) and not of MDPI and/or the editor(s). MDPI and/or the editor(s) disclaim responsibility for any injury to people or property resulting from any ideas, methods, instructions or products referred to in the content.